



Evidence for elevation-dependent warming from the Chinese Tianshan Mountains

Lu Gao^{1,2,3,4}, Haijun Deng^{1,2,3,4}, Xiangyong Lei³, Jianhui Wei⁵, Yaning Chen⁶, Zhongqin Li⁷, Miaomiao Ma⁸, Xingwei Chen^{1,2,3,4}, Ying Chen^{1,2,3,4}, Meibing Liu^{1,2,3,4}, Jianyun Gao⁹

5 ¹Institute of Geography, Fujian Normal University, Fuzhou 350007, China

²Fujian Provincial Engineering Research Center for Monitoring and Assessing Terrestrial Disasters, Fujian Normal University, Fuzhou 350007, China

³College of Geographical Sciences, Fujian Normal University, Fuzhou 350007, China

10 ⁴State Key Laboratory of Subtropical Mountain Ecology (Funded by the Ministry of Science and Technology and the Fujian province), Fujian Normal University, Fuzhou 350007, China

⁵Institute of Meteorology and Climate Research (IMK-IFU), Karlsruhe Institute of Technology, Campus Alpine, Garmisch-Partenkirchen 82467, Germany

⁶State Key Laboratory of Desert and Oasis Ecology, Xinjiang Institute of Ecology and Geography, Chinese Academy of Sciences, Urumqi 830011, China

15 ⁷State Key Laboratory of Cryospheric Sciences/Tianshan Glaciological Station, Northwest Institute of Eco-Environment and Resources, Chinese Academy of Sciences, Lanzhou 730000, China

⁸China Institute of Water Resources and Hydropower Research, Beijing 100038, China

⁹Fujian Key Laboratory of Severe Weather, Fuzhou 350001, China

Correspondence to: Lu Gao (l.gao@foxmail.com)

20 **Abstract.** The phenomenon that the warming rate of air temperature is amplified with elevation is termed elevation-dependent warming (EDW). It has been clarified that EDW can accelerate the retreat of glaciers and the melting of snow, which would have significant impacts on regional ecological environment. Owing to the lack of high-density ground observations in the high mountains, there is a widespread controversy on the existence of the EDW. Current evidences are mainly derived from some typical high mountains such as the Swiss Alps, the Colorado Rocky Mountains, the Tropical
25 Andes and the Tibetan Plateau/Himalayas. Rare evidences in other mountains have been reported, especially in arid regions. In this study, EDW features in the Chinese Tianshan Mountains (CTM) are detected using a unique high-resolution (1 km, 6-hourly) air temperature data set (CTMD). The results showed that there are significant EDW signals at different altitudes on different time scales. The warming rate of the minimum temperature in winter shows significant elevation dependence, especially above 4000 m. The greatest altitudinal gradient in the warming rate of maximum temperature is found above 2500
30 m in April. For the mean temperature, the warming rates in January, February and March show prominent EDW features but with different significances. Within the CTM, the Tolm Mountains, the eastern part of the Borokoonu Mountains, the Bogda Mountains and the Balikun Mountains are the representative regions that show significant EDW features on different time scales. This new evidence partly explains the accelerated melting of glaciers in spring in the CTM.



1 Introduction

35 The elevation-dependent warming (EDW) indicates that the warming rate of air temperature is amplified with elevation, especially in the high mountain regions. Normally, two criteria (regional warming amplification and altitude warming amplification) should be met concurrently to be recognized as a typical EDW phenomenon (Rangwala and Miller, 2012). The regional warming amplification means the warming rate of air temperature in a certain mountain is greater compared to other regions outside this mountain. The altitude warming amplification means the warming rate is greater in the high-
40 altitude areas than the low-altitude areas within the same mountain. However, owing to the high sensitivity of glaciers and snow to climate change, mountains are regarded as the outposts of global climate change (Sorg et al., 2012). Previous studies have reported the potential widespread existence of the elevation-dependent warming (EDW) phenomenon, which is an ideal early indicator of climate warming in mountain systems under global climate change (Dong et al., 2015). EDW could accelerate the changes in the mountain ecosystems, cryosphere systems, water cycles and biodiversity, leading to irreversible
45 and profound impacts on the regional ecological environment and socioeconomic development (Mountain Research Initiative EDW Working Group, 2015; Rangwala and Miller, 2012). Therefore, the detection and exploration of the spatial and temporal differentiation characteristics of EDW not only plays an inestimable and important role in the in-depth understanding of regional climate change and in improving the predictive ability of mountain climate, but also in maintaining the relative stability and ecological balance of these natural mountain ecosystems.

50 Current evidences for the EDW phenomenon mainly stem from multi-source data detections and regional climate models. The main data resources include ground meteorological stations, radiosonde, reanalysis, and remote sensing data. In general, from a regional perspective, the European Alps, Himalayas-Tibetan Plateau, South American Andes, and North American Rocky Mountains are hotspots for EDW studies (Wang et al., 2014; Thakuri et al., 2019; Guo et al., 2019; Pepin et al., 2019). From the perspective of the significance of EDW, the seasonal scale is more significant than the annual scale (Mountain
55 Research Initiative EDW Working Group, 2015; Rangwala and Miller, 2012). Furthermore, the warming rate of the minimum temperature is greater than that of the maximum and mean temperatures (Rangwala and Miller, 2012; Mountain Research Initiative EDW Working Group, 2015).

The results of global mountain detection based on multi-source observation data show that the warming trend of the annual mean temperature is more significant with rising elevation in the northern Tibetan Plateau, eastern Loess Plateau, Yunnan-
60 Guizhou Plateau, Appalachian Mountains, Southern Rocky Mountains, Alps, Andes, and Inner Mongolia Plateau (Wang et al., 2014). The warming rate has been found to be more intense in the high-altitude regions of Western Europe and Asia based on a global high-altitude observation data set (Diaz and Bradley, 1997). The significant EDW phenomenon of the annual maximum and minimum temperatures in the Alps has been detected based on ground observation sites (Beniston and Rebetez, 1996). The temperatures in the Alps at different altitudes show distinctly different seasonal trends. The minimum
65 temperature rises faster at high altitudes than at low altitudes (Jungo and Beniston, 2001). A significant EDW phenomenon



for the annual mean temperature in tropical alpine areas has been detected based on global radiosonde data (Seidel and Free, 2003). The warming trends for the maximum and minimum temperatures show significant elevation dependence in the 2000–4000 m altitude range of the Rocky Mountains (Diaz and Eischeid, 2007; Mcguire et al., 2012). The climate warming trend for the Qinghai-Tibet Plateau from 1961 to 1990 was proportional to the altitude, especially in winter (Liu and Hou, 70 1998). In the high-altitude areas (above 4000 m) of the Qinghai-Tibet Plateau, the increment in the mean temperature over four seasons and on the annual scale is greater than that in the low-altitude areas (Du, 2001); the temperature warming rate increases by $0.16\text{ }^{\circ}\text{C}\ 10\text{a}^{-1}$ for every 1 km increment in altitude (Wang et al., 2012). The satellite data also showed that climate warming on the Tibetan Plateau is altitude-dependent, especially at an altitude of 3000–4800 m (Yan and Liu, 2014).

Although many studies have detected EDW phenomena in different mountains globally, there is still widespread controversy 75 and no consensus has been reached on the existence of EDW. The main reason behind this is the scarcity of ground observation data, especially in mountains above 3000 m (Rangwala and Miller, 2012; Mountain Research Initiative EDW Working Group, 2015). Even the detection of EDW is different within the same mountain that uses different observations (i.e. different number of sites or different site locations). For example, some studies have shown a significant prevalence of EDW since the second half of the 20th century over the Tibetan Plateau (Liu et al., 2009; Rangwala et al., 2009). However, 80 an analysis claimed that the EDW over the Qinghai-Tibet Plateau is not significant based on the observations from 71 ground stations and 56 reanalysis grid data (You et al., 2010). Similarly, EDW has been found to be not significant at altitudes above 5000 m based on the observations from 25 ground stations and 0.5° grid data combined with WRF model simulations (Gao et al., 2018b). Although satellite data compensates for the deficiencies of ground observation stations to a large extent, the associated short time series, low spatial resolution, and large system errors limit the reliability of EDW 85 signal detection. It can be concluded that a uniform high-resolution air temperature dataset is the basic premise for accurate EDW detection.

As the largest independent latitudinal mountain system, the farthest mountain system from the ocean, and the largest mountain system in the arid regions of the world, the Tianshan Mountain system is extremely important for assessing the climate change and ecological environment in north-western China and the entire nation because of its special geographical 90 location and complex terrain (Chen et al., 2016). As the “water tower” of Central Asia, the Tianshan Mountain system not only breeds many rivers, but also produces a unique desert oasis ecosystem (Sorg et al., 2012; Chen et al., 2016). There are approximately 9035 glaciers with an area of $\sim 9225\text{ km}^2$ and water resources of 1011 km^3 in the Chinese Tianshan Mountains (CTM, Fig. 1) (Shi et al., 2009). However, in recent years, most glaciers in the CTM are in a state of accelerated degradation due to climate warming (Ding et al., 2006; Chen et al., 2016; Sorg et al., 2012). The warming rate in the CTM 95 has reached $0.32\text{--}0.42\text{ }^{\circ}\text{C}\ 10\text{a}^{-1}$ in the past 50 years, which is much higher than the national average (Gao et al., 2018a; Xu et al., 2018). However, EDW in the CTM still lacks systematic detection. Current research on climate warming in the CTM does not provide sufficient solid evidence for the EDW phenomenon. Therefore, in this study, EDW features in the CTM are



comprehensively and systematically detected based on a unique high-resolution (1 km, 6-hourly) air temperature dataset (hereafter referred to as CTMD) (Gao et al., 2018a). The present study reveals the EDW characteristics for different temperature indicators on different time scales.

2 Data and Methods

According to the two basic criteria for the diagnosis of mechanisms responsible for EDW, regional warming amplification and altitude warming amplification is detected, respectively. The former feature is compared with other regions, such as plateaus, mountains, and low-altitude areas (basins and plains), to detect whether the warming trend in the mountain is greater. The latter criterion focuses on the warming trend differences within the mountains (e.g., different altitude ranges), which is to determine whether warming amplification in the high-altitude areas is more significant than the low-altitude areas. To detect the regional warming amplification, a monthly temperature dataset at the 0.5° latitude-longitude grid (hereafter referred to as CMA05) over continental China from the China Meteorological Data Sharing Service System of the National Meteorological Information Centre was evaluated and compared with the CTMD. The CMA05 dataset was generated by integrating the data collected at high-density ground stations (approximately 2400 national meteorological observation stations) since 1961. The common time period 1979–2016 was extracted for the comparison.

Previous studies have shown that the ECMWF's third generation reanalysis product, ERA-Interim has a small large-scale error and it could capture the annual and seasonal climatologies very well (Gao et al., 2012, 2014, 2017). Because the system bias of ERA-Interim is mainly from the height discrepancy between ERA-Interim model height and observations (Gao et al., 2012, 2014, 2017). Thus, the bias could be significant reduced for local climate trend investigation via an appropriate elevation correction procedure. A robust approach based on internal vertical lapse rates derived from different ERA-Interim pressure levels was developed for downscaling 0.25° grid ERA-Interim temperature to 1 km grid (Gao et al., 2018a). This scheme is fully independent of meteorological stations via Equation (1).

$$T_{1km} = T_{ERA_{025}} + \Gamma \times \Delta h \quad (1)$$

$T_{ERA_{025}}$ is the original 6-hourly ERA-Interim 2-m temperature at 0.25° grid. Γ describes the ERA-Interim internal lapse rates derived from the temperatures and geopotential heights at different pressure levels. For example, $\Gamma_{500,700}$ indicates the lapse rate between 500 hPa and 700 hPa pressure level, which is calculated by the temperature differences divided by geopotential height differences between these two pressure levels. Δh is the height difference between ERA-Interim model height and 1 km grid. More information on the downscaling scheme and the CTMD could be found at Gao et al (2012, 2017, 2018a).

Therefore, the unique high-resolution (1 km, 6 h) air temperature dataset (CTMD) for the Chinese Tianshan Mountains from 1979 to 2016 is at 1 km spatial resolution (total 356133 grids) with a time step of 6-hourly at 00, 06, 12, and 18 UTC. This



dataset was validated by 24 meteorological stations on a daily scale, indicating a high reliability for the climatology trend investigations (Gao et al., 2018a). In this study, the 6-hourly data was aggregated to the minimum temperature (T_{min}), maximum temperature (T_{max}), and mean temperature (T_{mean}) on monthly, seasonal, and annual time scales. A standard linear regression was applied to calculate the warming rate in each grid from 1979–2016 for the CTMD and CMA05 datasets, respectively. The corresponding equation is given by:

$$y = \alpha x + \beta \quad (2)$$

where, y are the temperatures (T_{min} , T_{max} and T_{mean}) on different time scales, x is the time series from 1979–2016, and the fitting coefficient (slope) α indicates the warming rate.

To detect the altitude warming amplification within the CTM, the whole altitude range is divided into 14 groups with a 500 m interval. The 14 altitude groups are: <500 m, 500–1000 m, 1000–1500 m, 1500–2000 m, 2000–2500 m, 2500–3000 m, 3000–3500 m, 3500–4000 m, 4000–4500 m, 4500–5000 m, 5000–5500 m, 5500–6000 m, 6000–6500 m, and >6500 m. The number of grids in each group is 3139, 30810, 83018, 70229, 46545, 43400, 39579, 28256, 8789, 1666, 496, 150, 54, and 4, respectively. The standard linear regression was also used to assess the significance of EDW for different altitude groups. In such an analysis, y is the warming rate from 1979–2016 for each altitude group. Due to a different number of grids in each altitude group, the averaged warming rate of each group was used for the regression. x is the 14 altitude groups (natural positive integer 1 to 14). Thus, the fitting coefficient (slope) represents the magnitude of significance of EDW. The coefficient of determination (R^2) and confidence test (p -values) illustrate the goodness of the fit.

3 Results

3.1 Regional warming amplification of the CTM

The annual and seasonal temperature trends in the CTM are weaker than those over continental China with respect to the mean temperature (T_{mean}), maximum temperature (T_{max}), and minimum temperature (T_{min}), except during spring (Table 1). The warming rates in spring T_{max} and T_{min} both exceed $0.6 \text{ }^\circ\text{C } 10\text{a}^{-1}$, which is much higher than that of CMA05. The annual T_{min} shows the greatest warming trend with a rate of $0.347 \text{ }^\circ\text{C } 10\text{a}^{-1}$, followed by a T_{max} and T_{mean} warming rate of 0.323 and $0.245 \text{ }^\circ\text{C } 10\text{a}^{-1}$, respectively, in the CTM. While summer has a much higher gradient than autumn for T_{mean} and T_{min} , it shows a comparable rate for T_{max} . Winter has the lowest rates compared with other seasons for the three temperature trends, with even a decreasing trend ($-0.085 \text{ }^\circ\text{C } 10\text{a}^{-1}$) observed for T_{mean} . In general, T_{min} and T_{max} show comparable rates in spring. A more significant increment in T_{min} compared with T_{max} is observed in summer and autumn. However, the trends of CTMD are consistent with the national scale (CMA05), wherein T_{min} and T_{max} show higher rates than T_{mean} on the annual scale (Table 1).



However, the warming rate varies from month to month, which is more significant than that from season to season. All temperature trends are negative in January and December in the CTM, which is different from that over continental China. The decreasing rate is more significant in January than in December. It is worth noting that T_{max} decreases slightly in May, while T_{min} warms significantly at a rate of $0.624\text{ }^{\circ}\text{C}\ 10\text{a}^{-1}$ in the CTM. The largest warming rates are observed for both the CTM and land surface of China in March for all the temperature types. However, the CTM has a higher magnitude of warming rate. The warming trend is $1.339\text{ }^{\circ}\text{C}\ 10\text{a}^{-1}$, which is almost double than that over the whole of China (CMA05). Both rates exceed $0.8\text{ }^{\circ}\text{C}\ 10\text{a}^{-1}$ for T_{mean} and T_{min} in the CTM in March. April shows the second largest T_{max} and T_{mean} warming trends in the CTM, which are also higher than that over continental China. For T_{min} , May and June have rates greater than $0.6\text{ }^{\circ}\text{C}\ 10\text{a}^{-1}$. In general, a more significant increment in T_{min} is seen from March to June compared with the other months. March and April show remarkable warming trends for T_{max} and T_{mean} (Table 2). In the entire CTM, T_{min} warms faster than T_{max} and T_{mean} . In general, regional warming amplification is significant in March and June for all temperatures. The trend for T_{max} also increases faster in the CTM in February and April compared with the entire land surface of China. The warming rates in T_{mean} and T_{min} in the CTM are faster than the whole of China in April and May, respectively.

3.2 Warming amplification with altitude within the CTM

To detect the altitude warming amplification features in the mountain areas, the CTM is divided into 14 groups with a 500 m altitude interval. It is worth noting that the temperature trends in different elevation groups are significantly different compared with that of the entire CTM. Fig. 2 shows the T_{min} trends at different elevations from 1979–2016 for four representative months (January, February, April, and December). As the number of grids in each elevation group is different, the boxplots show the inner-quantile range (25% to 75%) and median value. Meanwhile, linear regression is applied based on the average values, which indicate the altitude dependence of the warming trend (i.e. the significance of EDW). In general, the EDW characteristics are significant for T_{min} in January, February, April, and December. All lines of best fit are at the 0.001 significance level ($p < 0.001$). The temperature trends are positive at altitudes higher than 5000 m, with the median values greater than $0\text{ }^{\circ}\text{C}\ 10\text{a}^{-1}$ above 4000 m in January (Fig. 2a). The median values of most elevation groups are above the reference line in February, although the corresponding line of fit has a lower slope (0.033) compared with that of January (Fig. 2b). The 75% quantile ranges of the trends for all elevation groups in April are higher than $0\text{ }^{\circ}\text{C}\ 10\text{a}^{-1}$ (Fig. 2c). All trends are positive for the regions nearly above 4000 m in April. The prevalence of EDW is most significant in December with the highest slope (0.064, $p < 0.001$). Although, most lower altitude grids ($< 4000\text{ m}$) show negative trends, the trends become positive at altitudes higher than 5000 m (Fig. 2d).

Although the slope (0.017) of the trend is not remarkable, a significant EDW trend ($p < 0.001$) is seen for T_{max} in March (Fig. 3a). Differing from that of April, August, and September, the same trend is observed for all elevation groups in March. Furthermore, all warming rates are greater than $0.8\text{ }^{\circ}\text{C}\ 10\text{a}^{-1}$. Significant elevation-dependent cooling can be found at the



altitude range of 0–2500 m for T_{max} in April. However, the temperature warming rate increases sharply (slope=0.069, $p<0.001$) with increment in the altitude from 2500 m to 7100 m. The median values are higher than $0.4\text{ }^{\circ}\text{C}\ 10\text{a}^{-1}$ (Fig. 3b).
190 Similar to April, EDW begins at a height of 4000–4500 m in August and September. However, the warming rates are greater in September with the most positive values compared with August (Figs. 3c and 3d). In general, while T_{max} warming is not widespread, it is more significant at higher elevations.

For T_{mean} , the EDW trend is most significant in January with the best significant level (slope=0.036, $p<0.001$, Fig. 3a). However, the warming rates in January are only slightly above $0\text{ }^{\circ}\text{C}\ 10\text{a}^{-1}$ at higher elevations. Although February and March
195 also show significant EDW at the 0.005 and 0.05 significant levels, respectively, the warming rates are much higher in March than in February with an average median value of approximately $0.8\text{ }^{\circ}\text{C}\ 10\text{a}^{-1}$ (Figs. 4b and 4c). Significant EDW occurs above an elevation of 4500 m in August (slope=0.037, Fig. 4d). The performances for all months and seasons are provided in the supplementary material (Fig. S1-S13).

3.3 Spatial distribution pattern of the warming trend over the CTM

200 To better detect the EDW features, four typical zones with high mountains (above 3000 m) were selected, namely Zone 1 (represented by the Tolm Mountains), Zone 2 (central Tianshan, including the eastern part of the Borokoonu Mountains), Zone 3 (represented by the Bogda Mountains), and Zone 4 (represented by the Balikun Mountains) (Fig. 5). The monthly minimum temperature trends of January in the higher altitude mountains are significantly greater than the surrounding low-altitude areas, especially in Zones 3 and 4 (Fig. 5a). The highest warming trend (exceeding $1.0\text{ }^{\circ}\text{C}\ 10\text{a}^{-1}$) is found around the
205 eastern Bogda Mountains (above 3000 m) in Zone 3. The lowland to the north of the Bogda Mountains shows a cooling trend (Fig. 5a). Zone 4 also shows a significant EDW phenomenon ($0.3\text{--}0.6\text{ }^{\circ}\text{C}\ 10\text{a}^{-1}$), wherein high mountains such as the Balikun are much warmer than the surrounding lowlands. Although the warming trend of Zone 1 is not as significant as that of Zones 3 and 4, compared with the Ili Valley (cooling trend), the warming rate is still remarkable ($\sim 0.4\text{ }^{\circ}\text{C}\ 10\text{a}^{-1}$). In December, the warming trend is more significant in Zone 1 compared with the other Zones (Fig. 5b). The trend in the Tolm
210 Mountains (exceeding $0.4\text{ }^{\circ}\text{C}\ 10\text{a}^{-1}$) is much higher than that in the Ili Valley (cooling trend), which is located in the northern part of Zone 1. The warming rate at high altitudes in Zone 3 is higher ($0.2\text{--}0.4\text{ }^{\circ}\text{C}\ 10\text{a}^{-1}$) than that in the lowlands. There is no obvious warming amplification in the high-altitude mountains of Zone 4 compared with the low-altitude areas (Fig. 5b). However, it is worth noting that even in the same mountainous area, such as in the Bogda Mountains in Zone 3, the warming rate in the east is significantly faster than that in the northwest.

215 The maximum temperature in March in the entire CTM warms significantly with rates ranging from 0.9 to $2.0\text{ }^{\circ}\text{C}\ 10\text{a}^{-1}$ (Fig. 6a). The highest warming rate can be observed in the western Ili Valley. However, all typical zones show strong EDW features. The areas above 4500 m in Zone 1 have trends higher than $1.4\text{ }^{\circ}\text{C}\ 10\text{a}^{-1}$. The smoothed contour of 3000 m corresponds to a distinct boundary in Zone 2. The temperature warming rates are almost higher than $\sim 1.5\text{ }^{\circ}\text{C}\ 10\text{a}^{-1}$ in the



220 areas above 3000 m, while the rates are smaller in the low altitude areas (Fig. 6a). The difference between the warming rates in the high-altitude and low-altitude areas is the most significant in Zone 3. The temperature warming trend on the hilltop of the Bogda Mountains is much higher than that at the foot of the mountains (Fig. 6a). The temperature warming rate in Zone 4 ranges from 1.3 to 1.6 °C 10a⁻¹. The trend differences between the high-altitude and low-altitude areas in Zone 4 are not as significant as those in Zone 3 (Fig. 6a). However, the warming rate on the hilltop is much higher than that in the neighbouring lowlands (Fig. 6a).

225 The spatial distribution of the maximum temperature in September shows a distinctive east-west differentiation. The warming rates in Zones 3 and 4 are greater than those in Zones 1 and 2 (Fig. 6b). The EDW feature is not significant in Zone 4. In contrast, the temperature in the high-altitude areas shows a slower warming trend (approximately 0.2–0.3 °C 10a⁻¹) than that in the low-altitude areas in Zone 3 (Fig. 6b). A slight EDW phenomenon can be seen in the Tolm Mountains in Zone 1. However, Zone 2 shows remarkable EDW in September compared with the other zones. Similar to March, areas above 3000
230 m warm faster than the lowlands, especially the Ili Valley (Fig. 6b). In summary, Zone 2 is found to be a significant EDW area in the maximum temperature for March and September.

Zones 1 and 4 tend to show the EDW phenomenon for the monthly mean temperature in January (Fig. 7a). The temperature decreases (by approximately -0.2 to -0.4 °C 10a⁻¹) in the Ili Valley but increases (approximately 0.05 to 0.15 °C 10a⁻¹) in the Tolm Mountains, especially in the high-altitude areas (Fig. 7a). Zone 4 warms faster than the regions outside the zone.
235 However, the warming trend is not significant in the high elevation areas compared with the lowlands within this zone (Fig. 7a). The temperatures show cooling trends in Zones 2 and 3. Nevertheless, the high-altitude areas are warmer than the low-altitude regions, especially in the Bogda Mountains of Zone 3 (Fig. 7a). The differences in the temperature trends of different terrains in Zone 2 are not indistinctive. The spatial distribution of the warming rate in February is similar to that in January. However, the trend in most areas of the CTM is positive (Fig. 7b). Zones 3 and 4 show obvious EDW phenomena in
240 February. The difference between the temperature warming rates in the high and low terrains of these two zones exceeds 0.2 °C 10a⁻¹. The trend in the high terrains of Zone 2 is greater than that in the valleys in the western part of the zone (eastern Ili Valley). However, the temperature in the south of the zone is warming faster than in the high mountains in the northern part of Zone 2 (Fig. 7b). The southwestern Tolm Mountains in Zone 1 are warming up faster than the north-eastern mountains. In general, the warming trend of mean temperature is not as dramatic and significant as that of the minimum and maximum
245 temperatures in the CTM. The spatial distribution of warming trends for all months and seasons could be found in the supplementary material (Fig. S14-S30).

4 Possible hypotheses and mechanisms

The air temperature changes are mainly affected by two aspects: one is the vertical energy exchange between the ground and atmosphere that leads to periodic changes on the daily and annual scales; the other is the temperature advection caused by



250 the movement of the cooling and heating masses, which leads to non-periodic changes. Numerous studies shown that the atmospheric circulation not only affects the latitude and zonality of climate via the zonal distribution of circulation, but also expands the influence range of sea-land and topography via the energy and water transportation (Dickinson, 1983; Harding et al., 2001). On a local scale, the ice and snow albedo, cloud cover, water vapor and radiation flux, and aerosols (including black carbon) are considered to be the main influence factors of EDW (Mountain Research Initiative EDW Working Group, 255 2015; Rangwala and Miller, 2012). However, whether clouds, water vapour and aerosols, the core mechanism is that they affect the absorption of solar short-wave radiation by the land surface and the long-wave radiation outward from the land surface (Shi et al., 2020; Zhang et al., 2018). The balance of surface energy is changed, which leads to increasing/decreasing near-surface air temperature. In other words, the surface energy balance is the key mechanism that affects seasonal and inter-annual changes of EDW (Rangwala and Miller, 2012).

260 Surface albedo is a comprehensive indicator of many factors that affect the surface energy balance. It is also the core factor and key variable that controls the surface energy budget (Dickinson, 1983; Harding et al., 2001; Wang et al., 2005). Surface albedo directly affects the absorption of solar radiation, which in turn affects the net surface radiation. Thus, it has an unusually significant effect on temperature regulation. Surface albedo determines the distribution of radiant energy between the land surface and atmosphere (Wang et al., 2005). Sometimes, its subtle changes would affect the energy budget of the 265 land-atmosphere system, which causes significant regional climate change (Harding et al., 2001; Dickinson, 1983).

Many factors such as terrain, vegetation cover, ice and snow, soil moisture, soil physical properties, and meteorological conditions could affect surface albedo (Zhang et al., 2018). For high mountain regions, vegetation cover and ice/snow cover are the two most important factors (Dickinson, 1983; Zhang et al., 2016; Zhang et al., 2018). They could change the surface albedo, soil moisture, net surface radiation, and the distribution ratio of sensible heat, latent heat, as well as soil heat flux 270 (Wang et al., 2002; Wang et al., 2005). Thus, surface albedo varies significantly with the seasonal variations of ice/snow cover and vegetation cover (Wang et al., 2002; Wang et al., 2005). For the whole CTM, small glaciers are more sensitive to the warming climate. The annual glacial retreat rate could be -2.3×10^3 kg m⁻² below 3000 m, especially in Zone 2 (Deng et al., 2019). The snow cover and its duration also show a decreasing trend (Sorg et al., 2012; Deng et al., 2019). Guo and Li (2015) found the decreasing trend of the ratio of snow fall to precipitation (S/P) in the CTM, especially in the four typical 275 zones 1 to 4 in this study. The changed S/P may be a cause of EDW in these zones. In sum, although many hypothetical mechanisms of EDW have received widespread attention, most of them are limited to phenomenon description and qualitative analysis. There is a lack of quantitative investigation on the core processes, dominant factors as well as temporal-spatial differences of EDW.



5 Discussion and Conclusions

280 Based on our analysis, it can be seen that the EDW phenomenon is very complicated for a large mountain system. It is hard
to arbitrarily judge the prevalence of EDW in a mountain system. Based on comprehensive quantitative analysis, we believe
that significant EDW signals exist in the CTM on local scales with respect to different temperature types. While previous
studies have mainly focused on the EDW of annual and seasonal temperatures, the monthly scale has not received sufficient
attention. However, seasonal temperatures cannot clearly reflect the EDW characteristics. In complex terrains, monthly
285 temperature changes are more significant, especially during season transitions. For example, rapid warming in March would
accelerate the melting of ice and snow, affecting the glaciers and regional water resources in the mountains.

Compared with the warming trend over the national land surface, the CTM is warming faster in spring. However, on a
monthly scale, the warming rates are more complicated. The warming gradients of the three temperature indicators (T_{min} ,
 T_{max} , and T_{mean}) in March and June in the CTM are higher than those over the entire national land surface on average.
290 Besides, the trends of T_{max} in February, T_{max} and T_{mean} in April, and T_{min} in May are also higher than the national
average. Therefore, EDW detection based on the monthly scale is more reasonable and accurate.

It cannot be simply concluded that the high-altitude areas are warming faster than the low-altitude areas. Quantitative
analysis is necessary to provide solid evidence of the EDW phenomenon. Via altitude grouping and a linear regression
model, we quantitatively determined the significance of EDW along with the detailed performance of the warming trends at
295 different altitudes. In the case of T_{min} , January, February, April, and December show significant EDW trends ($p < 0.001$).
The most significant EDW phenomenon is found in December. In other words, T_{min} is associated with strong EDW in
winter. The T_{min} warming rates for the areas above 5000 m are always positive, which could lead to the faster melting of
snow. For T_{max} , March, April, August, and September show different elevation-based sensitivities. The largest EDW trend
is found in March. However, the significant EDW phenomenon can only be found at altitudes above 2500 m, 4000 m, and
300 4500 m in April, August, and September, respectively. The T_{max} warming trends in March and April are always positive in
the CTM. January, February, and March also show significant EDW signal/phenomena over the entire CTM for T_{mean} . In
August, the EDW phenomenon can be detected in areas higher than 4500 m.

The CTM is a large mountain system consisting of many mountains. Therefore, EDW characteristics are diverse in different
mountains. The EDW of T_{min} in January is significant in the Bogda and Balikun Mountains, while it is significant in
305 December in the Tolm Mountains. For T_{max} in March, all the typical mountains exhibit EDW characteristics, especially the
central CTM and Bogda Mountains. A significant EDW signal of T_{max} is observed in September in the central CTM
(eastern part of the Borokoonu Mountains). The most significant EDW signal of T_{mean} is observed in the Tolm and Balikun
Mountains in January. The Bogda and Balikun Mountains exhibit significant EDW features in February.



Even in the same mountainous area, significantly different mechanisms of EDW are observed for different topographies,
310 altitudes, and seasons. Although many hypothetical mechanisms such as ice/snow albedo, cloud cover, water vapour and
radiant flux, and aerosols have received widespread attentions most of mechanisms are still limited to phenomenon
description and qualitative analysis. Quantitative research on the core processes, dominant factors, and spatial-temporal
differences in EDW remains inadequate. Future studies should focus on conducting in-depth quantitative research on the
mechanism of EDW based on regional climate models and field surveys, especially in Zones 1 and 2 with accelerating
315 glacier retreat.

6 Data availability

The data set is released at <https://doi.org/10.1594/PANGAEA.887700> with a Network Common Data Form (NetCDF)
format. The coverage of data set is 41.1814-45.9945 °N, 77.3484-96.9989 °E. The spatial resolution is 1km and the total
number of grid point is 818126 for a larger Chinese Tianshan Mountains region (which includes more surrounding areas.
320 This study used 356133 grids). The time step is 6-hourly at 00, 06, 12, and 18 UTC. The data set contains 288 NetCDF files
and one user guidance file. The monthly temperature data set at 0.5 ° latitude-longitude grid (CMA05) over the continental
China is provided by the China Meteorological Data Sharing Service System of the National Meteorological Information
Center (http://data.cma.cn/data/cdcdetail/dataCode/SURF_CLI_CHN_TEM_MON_GRID_0.5.html, last access: 28 June
2020).

325 Author contributions

L.G. designed the research and collected the data, H.D., X.L. and J.W. contributed to the data processing and analysis, L.G.
wrote the manuscript, and M.M., X.C., Y.N.C., Z.L., J.G., Y.C. and M.L. contributed to the discussion.

Competing interests

The authors declare that they have no conflict of interest.

330 Additional information

More analysis figures could be found in the Supplementary material.



Acknowledgements

This study was supported by the National Key Research and Development Program (2018YFE0206400 and 2018YFC1505805), National Natural Science Foundation of China (41877167 and 41807159), the Research and
335 Development Support Program of the China Institute of Water Resources and Hydropower Research (IWHR) (JZ0145B582017), the Scientific Projects from Fujian Provincial Department of Science and Technology (2019R1002-3), and the Outstanding Young Scientific Research Talents Cultivation Program, Education Department of Fujian Province. Dr. Jianhui Wei was supported financially by the German Research Foundation through funding of the AccHydro project (DFG-Grant KU 2090/11-1).

340 References

- Beniston, M., and Rebetez, M.: Regional behavior of minimum temperatures in Switzerland for the period 1979-1993, *Theoretical and Applied Climatology*, 53, 231-243, 1996.
- Chen, Y., Li, W., Deng, H., Fang, G., and Li, Z.: Changes in Central Asia's water tower: past, present and future, *Scientific Reports*, 6, 35458, 10.1038/srep35458, 2016.
- 345 Deng, H., Chen, Y., and Li, Y.: Glacier and snow variations and their impacts on regional water resources in mountains, *Journal of Geographical Sciences*, 29(1): 84-100, 2019.
- Diaz, H. F., and Bradley, R. S.: Temperature variations during the last century at high elevation sites, *Climatic Change*, 36, 253-279, 1997.
- Diaz, H. F., and Eischeid, J. K.: Disappearing “alpine tundra” Köppen climatic type in the western United States,
350 *Geophysical Research Letters*, 34, 2007.
- Ding, Y., Liu, S., Li, J., and Shangguan, D.: The retreat of glaciers in response to recent climate warming in western China, *Annals of Glaciology*, 43, 97-105, 2006.
- Dickinson, R. E.: Land surface processes and climate-surface albedos and energy balance, *Advances in Geophysics*, 25: 305-353, 1983.
- 355 Dong, D., Huang, G., Qu, X., Tao, W., and Fan, G.: Temperature trend–altitude relationship in China during 1963–2012, *Theoretical and Applied Climatology*, 122, 285-294, 2015.



- Du, J.: Change of temperature in Tibetan Plateau from 1961 to 2000, *Acta Geographica Sinica*, 56, 682-690, 2001. (in Chinese)
- Gao, L., Bernhardt, M., and Schulz, L.: Elevation correction of ERA-interim temperature data in complex terrain, *Hydrology and Earth System Sciences*, 16(12): 4661-4673, 2012.
- 360 Gao, L., Hao, L., and Chen, X.W.: Evaluation of ERA-interim monthly temperature data over the Tibetan Plateau, *Journal of Mountain Science*, 11(5): 1154-1168, 2014
- Gao, L., Bernhardt, M., Schulz, K., and Chen, X.W.: Elevation correction of ERA-Interim temperature data in the Tibetan Plateau, *International Journal of Climatology*, 37(9): 3540-3552, 2017.
- 365 Gao, L., Wei, J., Wang, L., Bernhardt, M., Schulz, K., and Chen, X.: A high-resolution air temperature data set for the Chinese Tian Shan in 1979–2016, *Earth System Science Data*, 10, 2097-2114, 2018a.
- Gao, Y., Chen, F., Lettenmaier, D. P., Xu, J., Xiao, L., and Li, X.: Does elevation-dependent warming hold true above 5000 m elevation? Lessons from the Tibetan Plateau, *npj Climate and Atmospheric Science*, 1, 2018b.
- Harding, R.J., Gryning, S.E., Halldin, S., and Lloyd, C.R.: Progress in understanding of land surface/atmosphere exchanges at high latitudes, *Journal of Geophysical Research*, 70, 5-18, 2001.
- 370 Mountain Research Initiative EDW Working Group: Elevation-dependent warming in mountain regions of the world, *Nature Climate Change*, 5, 424-430, 2015.
- Guo, L., and Li, L.: Variation of the proportion of precipitation occurring as snow in the Tian Shan Mountains, China, *International Journal of Climatology*, 35, 1379-1393, 2015.
- 375 Guo, D., Sun, J., Yang, K., Pepin, N., and Xu, Y.: Revisiting recent elevation-dependent warming on the Tibetan Plateau using satellite-based data sets, *Journal of Geophysical Research*, 124, 8511-8521, 2019.
- Jungo, P., and Beniston, M.: Changes in the anomalies of extreme temperature anomalies in the 20th century at Swiss climatological stations located at different latitudes and altitudes, *Theoretical and Applied Climatology*, 69, 1-12, 2001.
- L. Yan, and X. Liu: Has climatic warming over the Tibetan Plateau paused or continued in recent years?, *Journal of Earth, Ocean and Atmospheric Sciences*, 1, 13-28, 2014.
- 380



- Liu, X., and Hou, P.: Relationship between the climatic warming over the Qinghai -Xizang Plateau and its surrounding areas in recent 30 years and the elevation, *Advances in Climate Change Research*, 017, 245-249, 1998. (in Chinese)
- Liu, X., Cheng, Z., Yan, L., and Yin, Z.: Elevation dependency of recent and future minimum surface air temperature trends in the Tibetan Plateau and its surroundings, *Global and Planetary Change*, 68, 164-174, 2009.
- 385 Mcguire, C. R., Nufio, C. R., Bowers, M. D., and Guralnick, R. P.: Elevation-dependent temperature trends in the Rocky Mountain Front Range: changes over a 56- and 20-year record, *PLOS ONE*, 7, e44370, 2012.
- Pepin, N., Deng, H., Zhang, H., Zhang, F., Kang, S., and Yao, T.: An examination of temperature trends at high elevations across the Tibetan Plateau: the use of MODIS LST to understand patterns of elevation-dependent warming, *Journal of Geophysical Research*, 124, 5738-5756, 2019.
- 390 Rangwala, I., Miller, J. R., and Xu, M.: Warming in the Tibetan Plateau: possible influences of the changes in surface water vapor, *Geophysical Research Letters*, 36, L06703, 2009.
- Rangwala, I., and Miller, J. R.: Climate change in mountains: a review of elevation-dependent warming and its possible causes, *Climatic Change*, 114, 527-547, 2012.
- Seidel, D. J., and Free, M.: Comparison of lower-tropospheric temperature climatologies and trends at low and high
395 elevation radiosonde sites, *Climatic Change*, 59, 53-74, 2003.
- Shi, Y., Liu, C., and Kang, E.: The glacier inventory of China, *Annals of Glaciology*, 50, 1-11, 2009.
- Shi, T. L., Pu, W., Zhou, Y., Cui, J. C., Zhang, D. Z., and Wang, X.: Albedo of Black Carbon-Contaminated Snow Across Northwestern China and the Validation With Model Simulation, *Journal of Geophysical Research: Atmospheres*, 125, 2020.
- Sorg, A., Bolch, T., Stoffel, M., Solomina, O. N., and Beniston, M.: Climate change impacts on glaciers and runoff in Tien
400 Shan (Central Asia), *Nature Climate Change*, 2(10), 725-731, 2012.
- Thakuri, S., Dahal, S., Shrestha, D., Guyennon, N., Romano, E., Colombo, N., and Salerno, F.: Elevation-dependent warming of maximum air temperature in Nepal during 1976–2015, *Atmospheric Research*, 228, 261-269, 2019.
- Wang, K. C., Wang, P. C., Liu, J. M., Sparrow, M., Haginoya, S., and Zhou, X. J.: Variation of surface albedo and soil thermal parameters with soil moisture content at a semi-desert site on the western Tibetan Plateau, *Boundary-Layer
405 Meteorology*, 116(1), 117-129, 2005.



- Wang, P., Tang, G., Cao, L., Liu, Q., and Ren, Y.: Surface air temperature variability and its relationship with altitude and latitude over the Tibetan Plateau in 1981-2010, *Advances in Climate Change Research*, 8, 313-319, 2012. (in Chinese)
- Wang, Q., Fan, X., and Wang, M.: Recent warming amplification over high elevation regions across the globe, *Climate Dynamics*, 43, 87-101, 2014.
- 410 Wang, S.S., Grant, R.F., Verseghy, D.L., and Black, T.A.: Modelling carbon dynamics of boreal forest ecosystems using the Canadian Land Surface Scheme, *Climatic Change*, 55(4), 451-477, 2002.
- Zhang, C., Lu, D., Chen, X., Zhang, Y., Maisupova, B., and Tao, Y.: The spatiotemporal patterns of vegetation coverage and biomass of the temperate deserts in Central Asia and their relationships with climate controls, *Remote Sensing of Environment*, 175, 271-281, 2016.
- 415 Zhang, Y. L., Kang, S. C., Sprenger, M., Cong, Z. Y., Gao, T. G., Li, C. L., Tao, S., Li, X. F., Zhong, X. Y., Xu, M., Meng, W. J., Neupane, B., Qin, X., and Sillanpaa, M.: Black carbon and mineral dust in snow cover on the Tibetan Plateau, *The Cryosphere*, 12(2), 413-431, 2018.
- Xu, M., Kang, S., Wu, H., and Yuan, X.: Detection of spatio-temporal variability of air temperature and precipitation based on long-term meteorological station observations over Tianshan Mountains, Central Asia, *Atmospheric Research*, 203, 141-420 163, 2018.
- You, Q., Kang, S., Pepin, N., Flugel, W., Yan, Y., Behrawan, H., and Huang, J.: Relationship between temperature trend magnitude, elevation and mean temperature in the Tibetan Plateau from homogenized surface stations and reanalysis data, *Global and Planetary Change*, 71, 124-133, 2010.
- Zhang, C., Lu, D., Chen, X., Zhang, Y., Maisupova, B., and Tao, Y.: The spatiotemporal patterns of vegetation coverage and biomass of the temperate deserts in Central Asia and their relationships with climate controls, *Remote Sensing of Environment*, 175, 271-281, 2016.
- 425 Zhang, Y. L., Kang, S. C., Sprenger, M., Cong, Z. Y., Gao, T. G., Li, C. L., Tao, S., Li, X. F., Zhong, X. Y., Xu, M., Meng, W. J., Neupane, B., Qin, X., and Sillanpaa, M.: Black carbon and mineral dust in snow cover on the Tibetan Plateau, *The Cryosphere*, 12(2), 413-431, 2018.

430



Table 1. Annual and seasonal temperature trends ($^{\circ}\text{C } 10\text{a}^{-1}$) in the CTM (based on CTMD) and continental China (based on CMA05) from 1979–2016.

	CTMD			CMA05		
	Tmin	Tmean	Tmax	Tmin	Tmean	Tmax
Spring	<u>0.633</u>	<u>0.522</u>	<u>0.640</u>	0.557	0.518	0.513
Summer	0.441	0.342	0.266	0.472	0.378	0.388
Autumn	0.302	0.200	0.270	0.551	0.420	0.458
Winter	0.014	-0.085	0.115	0.432	0.327	0.361
Annual	0.347	0.245	0.323	0.503	0.411	0.430

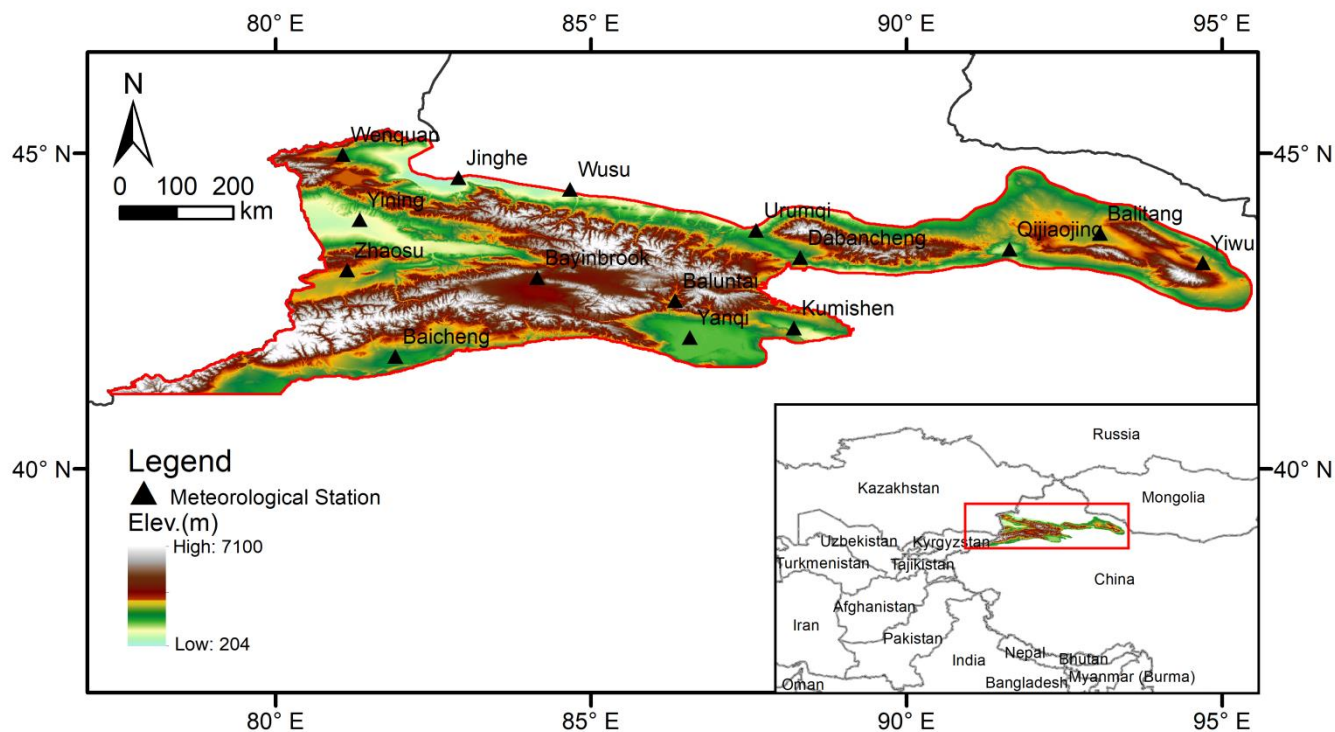
Note: the bold and underlined value indicates a greater warming trend in the CTM than continental China



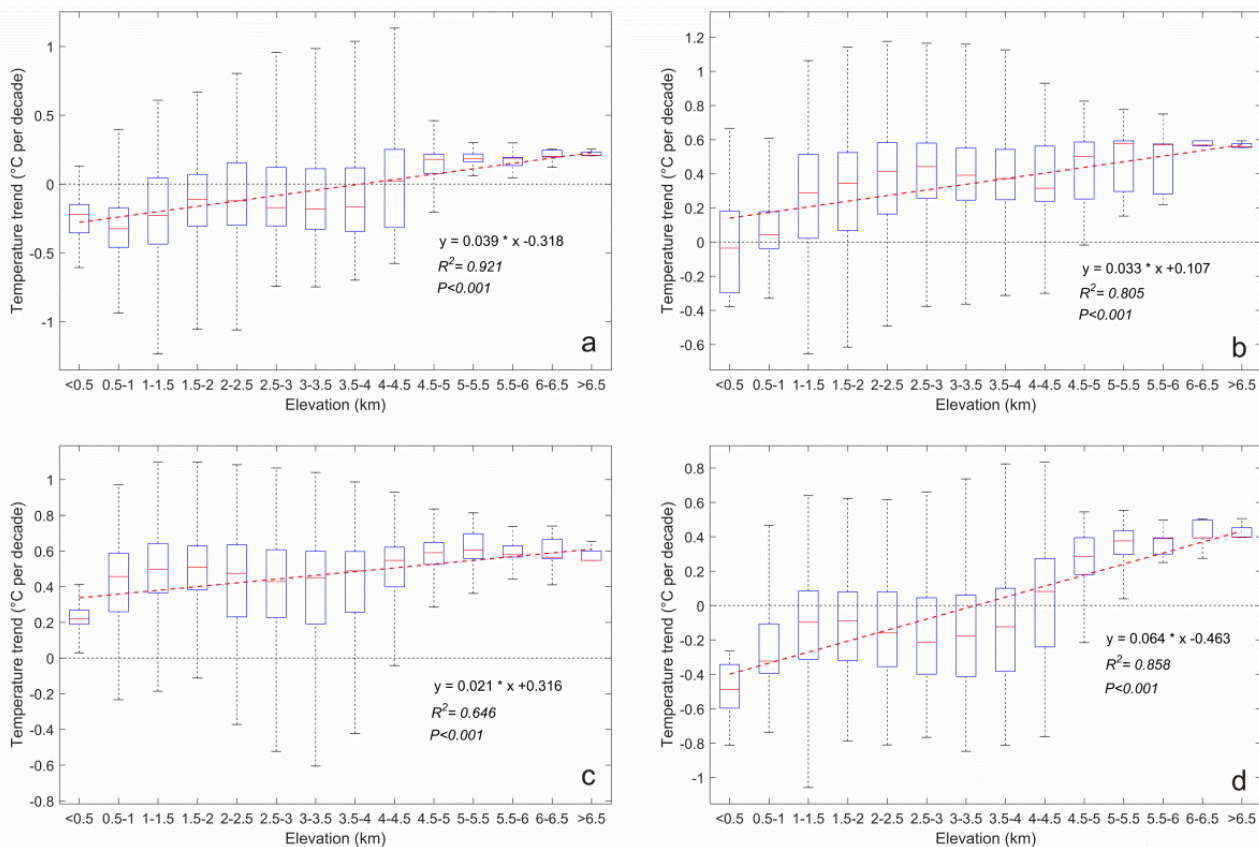
435 **Table 2. Monthly temperature trends ($^{\circ}\text{C } 10\text{a}^{-1}$) in the CTM (based on CTMD) and the continental China (based on CMA05) from 1979–2016.**

	CTMD			CMA05		
	Tmin	Tmean	Tmax	Tmax	Tmean	Tmin
January	-0.133	-0.269	-0.235	0.343	0.212	0.256
February	0.313	0.177	<u>0.605</u>	0.558	0.549	0.523
March	<u>0.835</u>	<u>0.818</u>	<u>1.339</u>	0.651	0.752	0.672
April	0.441	<u>0.537</u>	<u>0.664</u>	0.547	0.516	0.522
May	<u>0.624</u>	0.211	-0.082	0.475	0.284	0.345
June	<u>0.752</u>	<u>0.476</u>	<u>0.422</u>	0.516	0.344	0.390
July	0.227	0.331	0.280	0.472	0.416	0.411
August	0.342	0.217	0.095	0.429	0.375	0.363
September	0.246	0.237	0.330	0.559	0.495	0.486
October	0.273	0.180	0.227	0.524	0.398	0.434
November	0.386	0.183	0.252	0.569	0.368	0.455
December	-0.137	-0.164	-0.025	0.394	0.219	0.303

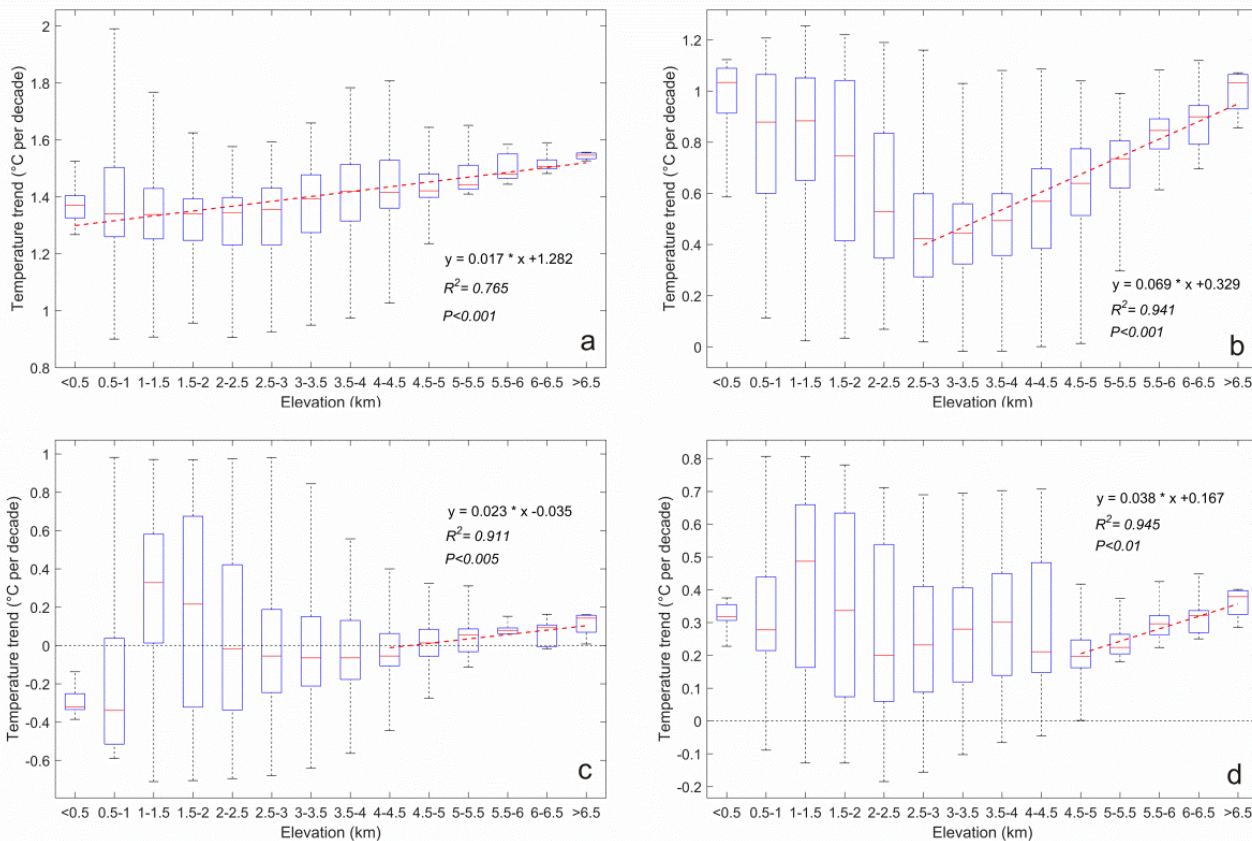
Note: the bold and underlined value indicates a greater warming trend in the CTM than continental China



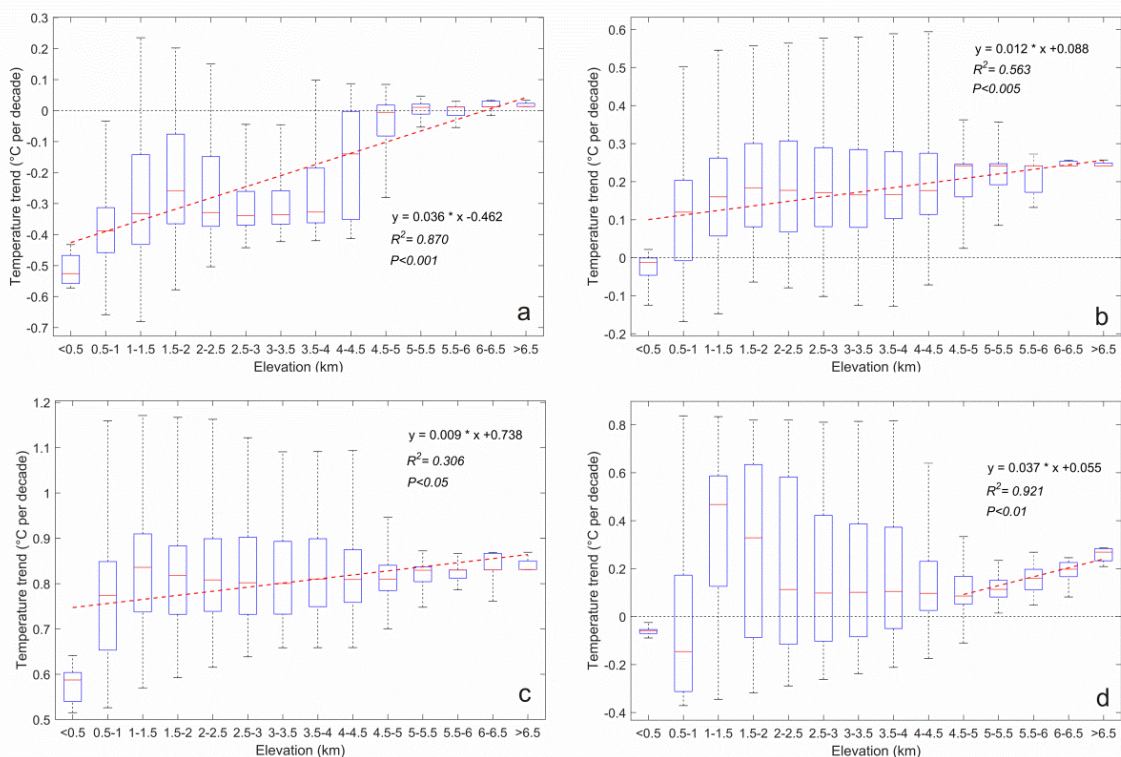
440 **Figure1:** Location of the Chinese Tianshan Mountains (CTM).The elevation ranges from 204 m to 7100 m a.s.l., with a DEM resolution of 1 km.



445 **Figure 2: Box plots of monthly minimum temperature trends in different elevations from 1979–2016. (a) January, (b) February, (c) April, and (d) December. Thick horizontal lines in boxes show the median values. Boxes indicate the inner-quantile range (25% to 75%) and the whiskers show the full range of the values. The red dashed lines represent the significance of EDW.**



450 **Figure 3: Box plots of monthly maximum temperature trends in different elevations from 1979–2016. (a) March, (b) April, (c) August, and (d) September. Thick horizontal lines in boxes show the median values. Boxes indicate the inner-quantile range (25% to 75%) and the whiskers show the full range of the values. The red dashed lines represent the significance of EDW.**



455

Figure 4: Box plots of monthly mean temperature trends in different elevations from 1979–2016. (a) January, (b) February, (c) March, and (d) August. Thick horizontal lines in boxes show the median values. Boxes indicate the inner-quartile range (25% to 75%) and the whiskers show the full range of the values. The red dashed lines represent the significance of EDW.

460

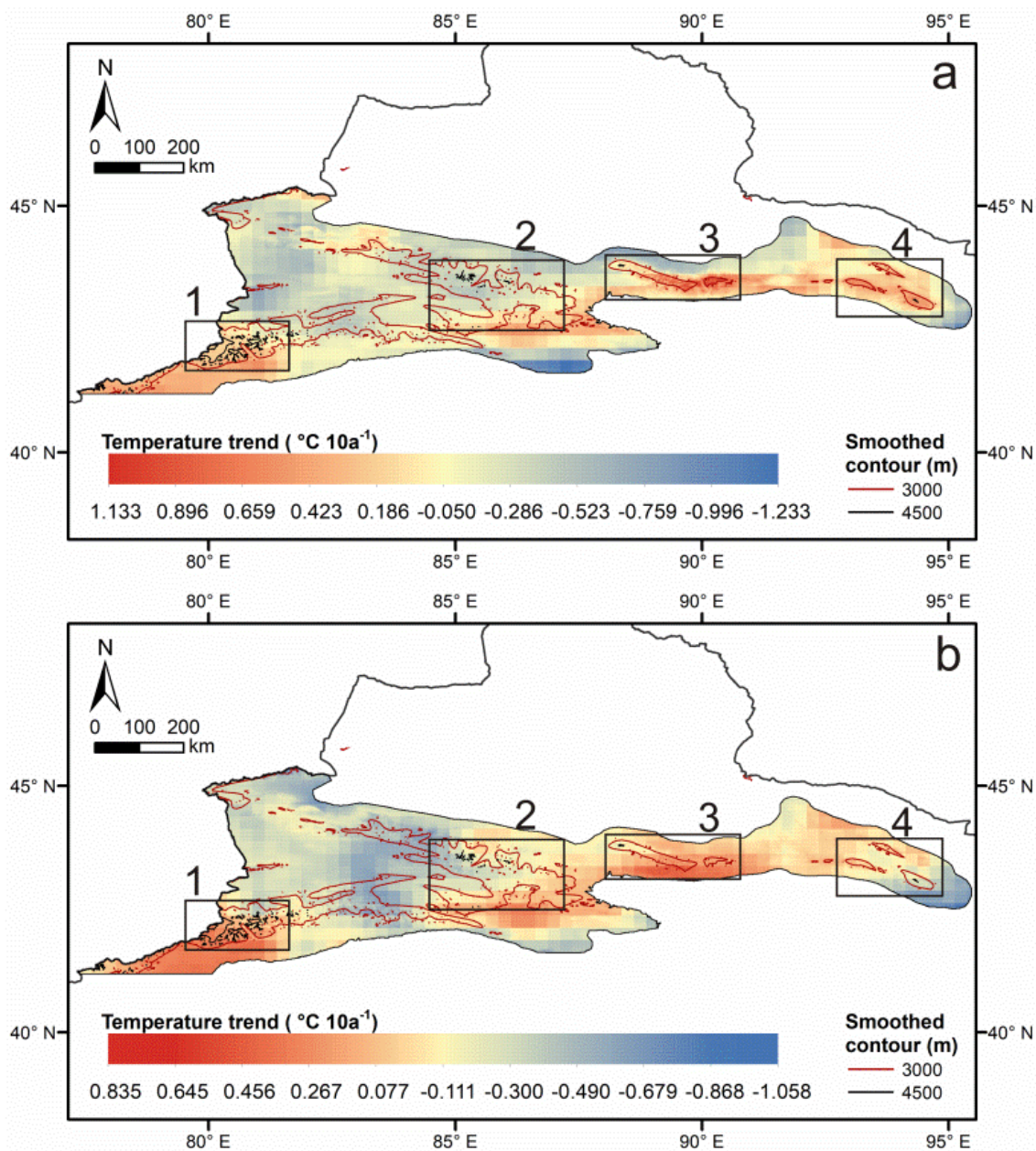
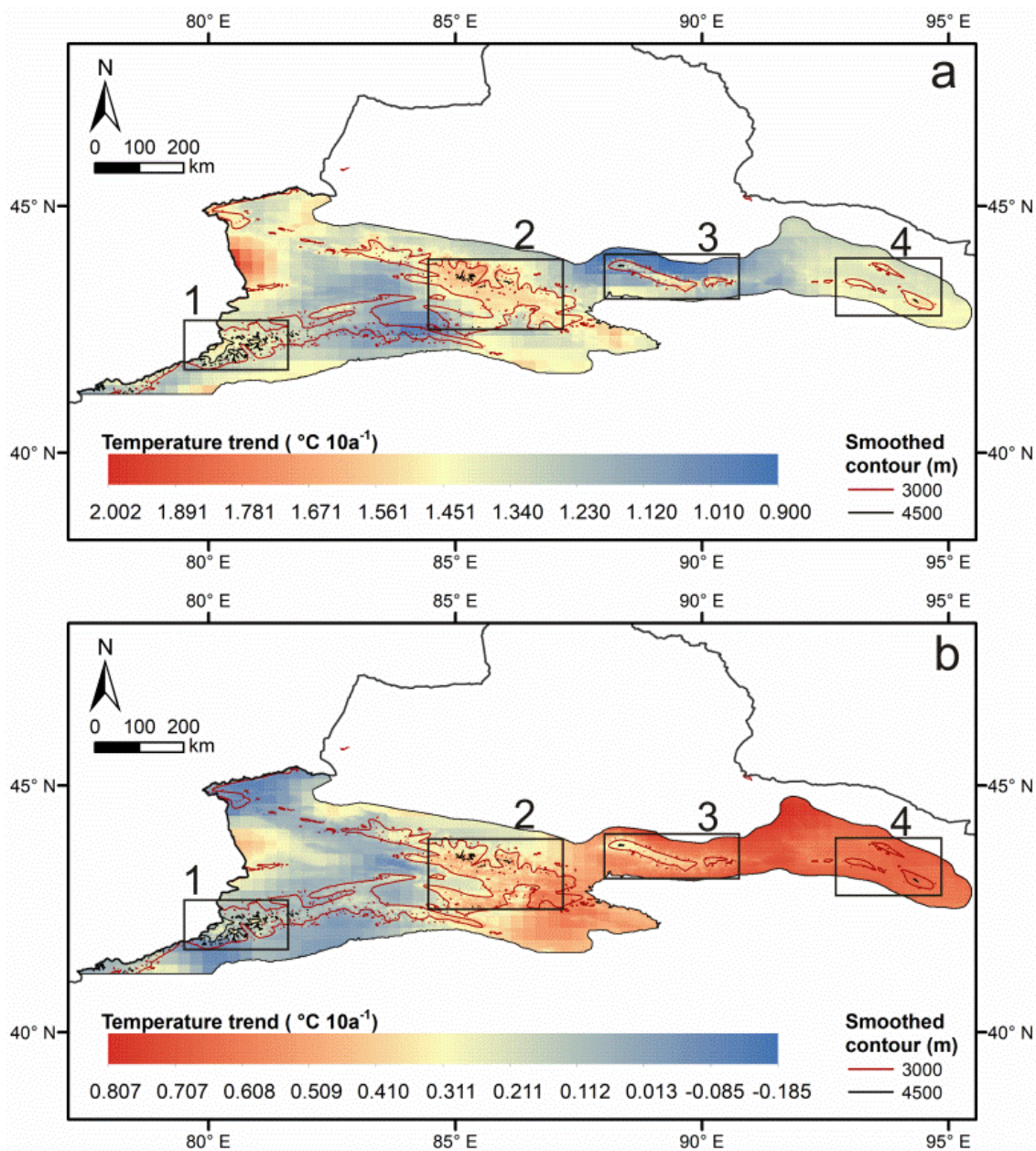


Figure 5: Monthly minimum temperature trends (a) January and (b) December for the entire CTM from 1979–2016.



465 **Figure 6: Monthly maximum temperature trends (a) March and (b) September for the entire CTM from 1979–2016.**

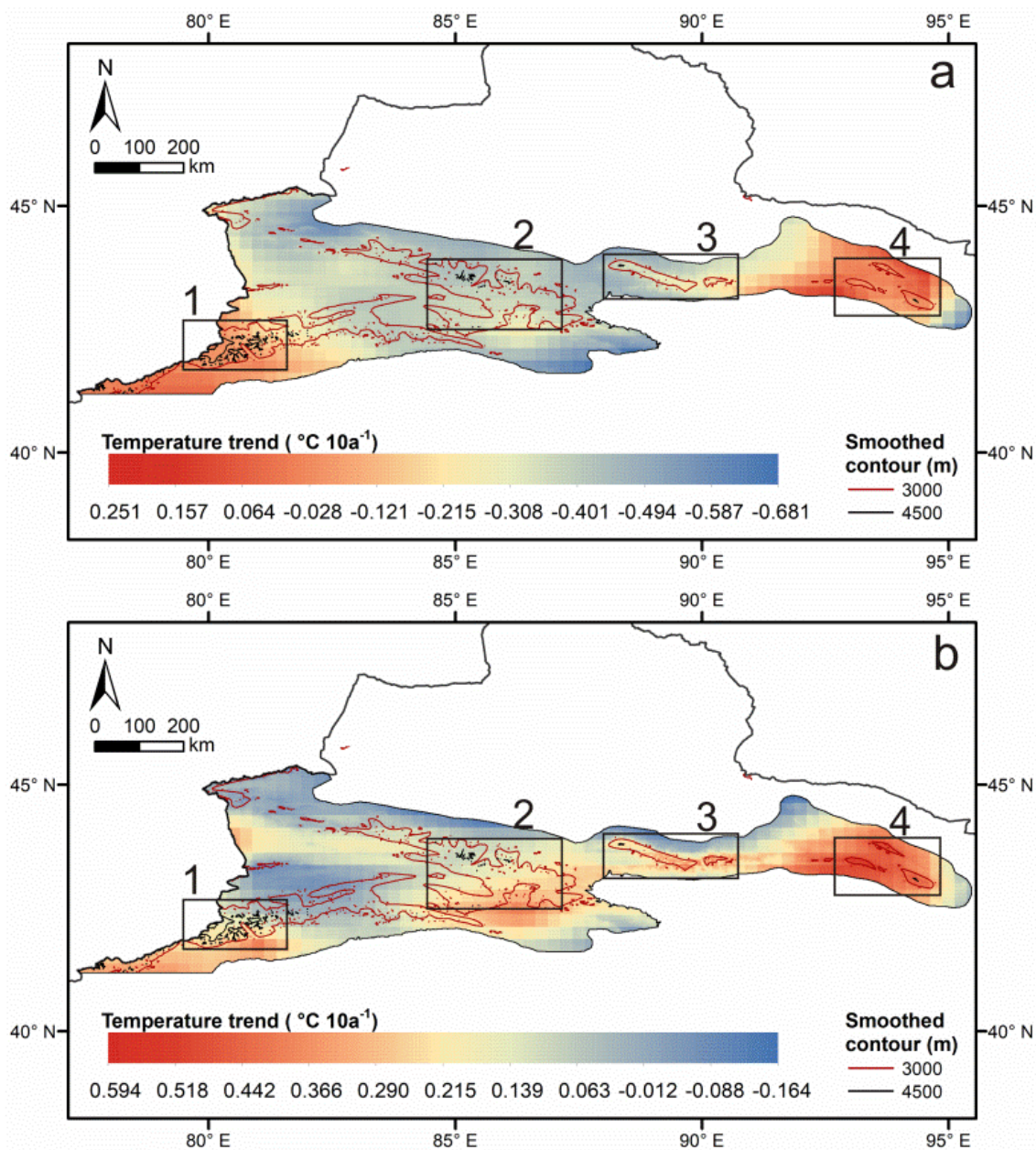


Figure 7: Monthly mean temperature trends (a) January and (b) February for the entire CTM from 1979–2016.